CO$_2$ laser micromachining of nanocrystalline diamond films grown on doped silicon substrates

JENS RICHTER,[1,5] ALY ABDOU,[2,5] OLIVER A. WILLIAMS,[3] JEREMY WITZENS,[1] AND MAZIAR P. NEZHAD[2,4,*]

[1]Institute of Integrated Photonics, RWTH Aachen University, Sommerfeldstrasse 24, D-52074 Aachen, Germany
[2]School of Electronic Engineering, Bangor University, LL57 1UT, UK
[3]School of Physics and Astronomy, Cardiff University, Queen's Buildings, The Parade, Cardiff CF24 3AA, UK
[4]Qualcomm Institute, University of California San Diego, La Jolla, CA 92093, USA
[5]Contributed equally
*maziar@bangor.ac.uk

Abstract: We demonstrate that nanocrystalline diamond films grown on highly doped silicon substrates can be patterned using a CO$_2$ laser operating at a wavelength of 10.6 μm, where both low doped silicon and diamond exhibit negligible optical absorption. The patterning is initiated by free carrier absorption in the silicon substrate and further enhanced by the thermal runaway effect, which results in surface heating in the silicon substrate and subsequent thermal ablation of the diamond film in an oxygen rich atmosphere. Using this approach, micron-scale grating and dot patterns are patterned in thin film diamond. The localized heating is simulated and analyzed using concurrent optical and thermal finite element modelling. The laser patterning method described here offers a cost effective and rapid solution for micro-structuring diamond films.

References and links

1. I. Aharonovich, A. D. Greentree, and S. Prawer, "Diamond photonics," Nat. Photonics **5**(7), 397–405 (2011).
2. P. Rath, S. Ummethala, C. Nebel, and W. H. P. Pernice, "Diamond as a material for monolithically integrated optical and optomechanical devices," Phys. Status Solidi., A Appl. Mater. Sci. **212**(11), 2385–2399 (2015).
3. A. V. Sumant, O. Auciello, M. Liao, and O. A. Williams, "MEMS/NEMS based on mono-, nano-, and ultrananocrystalline diamond films," MRS Bull. **39**(06), 511–516 (2014).
4. A. Aleksov, M. Kubovic, M. Kasu, P. Schmid, D. Grobe, S. Ertl, M. Schreck, B. Stritzker, and E. Kohn, "Diamond-based electronics for RF applications," Diamond Related Materials **13**(2), 233–240 (2004).
5. M. P. Hiscocks, C. J. Kaalund, F. Ladouceur, S. T. Huntington, B. C. Gibson, S. Trpkovski, D. Simpson, E. Ampem-Lassen, S. Prawer, and J. E. Butler, "Reactive ion etching of waveguide structures in diamond," Diamond Related Materials **17**(11), 1831–1834 (2008).
6. A. Masood, M. Aslam, M. Tamor, and T. Potter, "Techniques for Patterning of CVD Diamond Films on Non-Diamond Substrates," J. Electrochem. Soc. **138**(11), L67–L68 (1991).
7. V. I. Konov, T. V. Kononenko, and V. V. Kononenko, "Laser Micro- and Nanoprocessing of Diamond Materials," in *Optical Engineering of Diamond*, R. P. Mildren and J. R. Rabeau, eds. (Wiley-VCH, 2013), pp. 385–443.
8. S. Preuss and M. Stuke, "Subpicosecond ultraviolet laser ablation of diamond: Nonlinear properties at 248 nm and time-resolved characterization of ablation dynamics," Appl. Phys. Lett. **67**(3), 338–340 (1995).
9. T. V. Kononenko, V. G. Ralchenko, I. I. Vlasov, S. V. Garnov, and V. I. Konov, "Ablation of CVD diamond with nanosecond laser pulses of UV–IR range," Diamond Related Materials **7**(11-12), 1623–1627 (1998).
10. S. Albin, A. D. Cropper, L. C. Watkins, C. E. Buvik, and A. M. Buoncristiani, "Laser Damage Threshold Of Diamond Films," Opt. Eng. **28**(3), 283281 (1989).
11. V. V. Migulin, V. G. Ralchenko, and Y. J. Baik, "Oxygen-assisted laser cutting and drilling of CVD diamond," in *Lasers in Synthesis, Characterization, and Processing of Diamond*, V. I. Konov and V. G. Ralchenko, eds. (SPIE, 1997), Vol. 3484, pp. 175–179.

12. M. Rothschild, C. Arnone, and D. J. Ehrlich, "Excimer-laser etching of diamond and hard carbon films by direct writing and optical projection," J. Vac. Sci. Technol. B **4**(1), 310–314 (1986).
13. V. G. Ral'chenko, K. G. Korotushenko, A. A. Smolin, and E. N. Loubnin, "Fine patterning of diamond films by laser-assisted chemical etching in oxygen," Diamond Related Materials **4**(7), 893–896 (1995).
14. R. P. Mildren, "Intrinsic Optical Properties of Diamond," in *Optical Engineering of Diamond*, R. P. Mildren and J. R. Rabeau, eds. (Wiley-VCH, 2013), pp. 1–34.
15. B. J. M. Hausmann, B. Shields, Q. Quan, P. Maletinsky, M. McCutcheon, J. T. Choy, T. M. Babinec, A. Kubanek, A. Yacoby, M. D. Lukin, and M. Lončar, "Integrated Diamond Networks for Quantum Nanophotonics," Nano Lett. **12**(3), 1578–1582 (2012).
16. P. Rath, N. Gruhler, S. Khasminskaya, C. Nebel, C. Wild, and W. H. P. Pernice, "Waferscale nanophotonic circuits made from diamond-on-insulator substrates," Opt. Express **21**(9), 11031–11036 (2013).
17. M. Blomberg, K. Naukkarinen, T. Tuomi, V.-M. Airaksinen, M. Luomajärvi, and E. Rauhala, "Substrate heating effects in CO2 laser annealing of ion-implanted silicon," J. Appl. Phys. **54**(5), 2327–2328 (1983).
18. I. W. Boyd, T. D. Binnie, J. I. B. Wilson, and M. J. Colles, "Absorption of infrared radiation in silicon," J. Appl. Phys. **55**(8), 3061–3063 (1984).
19. A. Yariv and P. Yeh, *Photonics: Optical Electronics in Modern Communications* (Oxford University Press, 2007).
20. E. L. H. Thomas, G. W. Nelson, S. Mandal, J. S. Foord, and O. A. Williams, "Chemical mechanical polishing of thin film diamond," Carbon **68**, 473–479 (2014).
21. O. A. Williams, "Nanocrystalline diamond," Diamond Related Materials **20**(5-6), 621–640 (2011).
22. R. K. Endo, Y. Fujihara, and M. Susa, "Calculation of the density and heat capacity of silicon by molecular dynamics simulation," High Temp. High Press. **35-36**(5), 505–511 (2003).
23. J. R. Meyer, M. R. Kruer, and F. J. Bartoli, "Optical heating in semiconductors: Laser damage in Ge, Si, InSb, and GaAs," J. Appl. Phys. **51**(10), 5513–5522 (1980).
24. N. M. Ravindra, B. Sopori, O. H. Gokce, S. X. Cheng, A. Shenoy, L. Jin, S. Abedrabbo, W. Chen, and Y. Zhang, "Emissivity Measurements and Modeling of Silicon-Related Materials: An Overview," Int. J. Thermophys. **22**(5), 1593–1611 (2001).
25. D. C. Harris, *Development of Chemical-Vapor-Deposited Diamond for Infrared Optical Applications. Status Report and Summary of Properties* (Naval Air Warfare Center Weapons Div China Lake CA, 1994).

1. Introduction

Diamond is a wide bandgap semiconductor with unique optical, mechanical and thermal properties. Advances in material growth and wafer bonding techniques have enabled the integration of diamond thin films with standard semiconductor materials such as silicon (Si) and silicon-on-insulator (SOI), leading to an increasing range of applications. In particular, nanocrystalline thin film diamond layers, which can be seeded and grown on a variety of substrates, are finding increasing applications in photonics, MEMS and electronics [1–4]. Patterning such thin films is a fundamental processing step in any of these applications. Patterning of thin film diamond has been achieved with a variety of techniques including oxygen based reactive ion etching [5], pre-patterning of the seed layer [6] and laser micromachining [7].

Laser patterning of diamond is based on one of two main processes, vaporization ablation (physical removal), or laser induced chemical etching [7]. Vaporization ablation occurs when the surface of diamond is heated to above the sublimation temperature of carbon (≈4000 °K). This type of patterning can be carried out in non-reactive environments such as argon gas or vacuum using high peak power pulsed lasers [8,9]. Laser induced chemical etching, on the other hand, occurs at much lower temperatures but requires the presence of a reactive gas such as oxygen. In this case, the etching process is initiated through graphitization of diamond at about 1000 °K [7]. In the process of graphitization the mean atomic distance between the carbon atoms increases. Therefore graphitization is initiated at locations where free space is available for volume expansion, namely the surface of the diamond film. This surface graphite layer has higher optical absorption and reduced thermal conductivity compared to diamond and, under the right conditions, will absorb an incoming laser beam and continue to heat up to the point of chemically reacting with oxygen (combustion). During this process the surface of diamond will re-graphitize, resulting in sustained removal of diamond at the location of the laser beam. Patterning diamond with high peak power pulsed lasers in a non-inert environment such as oxygen can be due to a combination of vaporization and chemical etching.

It has been previously observed that laser beams with high peak powers but with photon energies below the bandgap of diamond can induce chemical etching of diamond thin films grown on silicon substrates. This is somewhat unexpected, given the high transparency of diamond at these wavelengths. Albin et al. [10] observed laser induced damage of polycrystalline diamond films grown on silicon, using a 1064 nm 50 nanosecond pulsed Nd:YAG laser beam at a fluence of 1.5 J/cm^2. At the same time they noticed that free standing films of diamond have much higher damage thresholds, about 7 J/cm^2. They attribute this difference to substrate surface modification and thermally induced mechanical stress in the diamond film. Migulin et al. [11] report patterning of diamond on silicon under similar illumination conditions in an oxygen-rich environment. Kononenko et al. [9] report ablation of free standing chemical vapor deposited (CVD) diamond with nanosecond pulses at 1078 nm, 539 nm and 270 nm. They also note insensitivity of the ablation rate to wavelength. In both [9] and [11], the patterning is ascribed to surface graphitization and absorption of the laser beam by the graphitized layer [12].

It is reasonable to assume that the high intensity of a pulsed Q-switched or mode-locked laser beam can initiate the graphitization process, either directly (through multiphoton, multiphonon or surface state absorption processes) or indirectly (through impurity absorption and localized heating in the bulk of the diamond). However, in some instances patterning has also been demonstrated with continuous wave (CW) laser beams at relatively low peak powers. Ral'chenko et al. demonstrate patterning of grooves and holes on polycrystalline diamond films grown on silicon and molybdenum using a 2 watt CW argon laser operating at 488 nm [13]. They also ascribe this etching to surface graphitization, however it is not clear how this would be initiated at this (relatively) low optical power.

In this work we suggest another pathway to explain laser induced chemical etching in such thin film structures. We believe that this is especially relevant to low peak power CW cases, however it is very likely that the same process plays an important role in the case of pulsed laser etching of diamond. We contend that the role of the substrate has been neglected in most (if not all) reports of laser induced chemical etching of diamond thin films on silicon substrates. In particular we show that, under certain conditions, localized substrate heating can be the dominant factor for initiating graphitization. In this scenario, the laser beam does not directly graphitize the surface of the diamond film, but rather the underlying substrate absorbs the incoming beam which then heats up the adjacent area on the diamond film to temperatures above 1000 °K, leading to surface graphitization. Through thermooptic simulations and laser machining experiments we demonstrate that this effect holds even for wavelengths far from the band edges of diamond and silicon, in this case the CO_2 laser operating at 10.6 μm.

2. Infrared optical properties of diamond and silicon at high temperatures

Our experiments involve the laser patterning of diamond films grown on silicon wafers using a CO_2 laser. The CW CO_2 laser, operating at 10.6 μm, is a widely used workhorse of the laser micromachining industry due to its high optical power and relatively low cost of ownership. At first glance it would seem that, given the much lower photon energy of the CO_2 laser compared to the band gaps of silicon and diamond, patterning diamond films with a CO_2 laser beam will not be possible. However, as we will show, this can be facilitated through the free carriers present in doped silicon substrates.

We first present an overview of the infrared optical properties of both materials at elevated temperatures at the wavelength of interest. Crystalline diamond has a bandgap of 5.47 eV, a refractive index of 2.38 and a transparency window covering the UV to 20 μm [14], with some heightened absorption between 2.6 and 6.2 microns due to lattice absorption. These superior transmission properties have led to the use of diamond in a variety of infrared optical applications, such as high power infrared transmission windows. Nanophotonic diamond based waveguide platforms have also been developed, such as integrated photonic

circuits using wafer-bonded hybrid diamond on oxide substrates [15] or CVD nanocrystalline diamond grown on oxide [16].
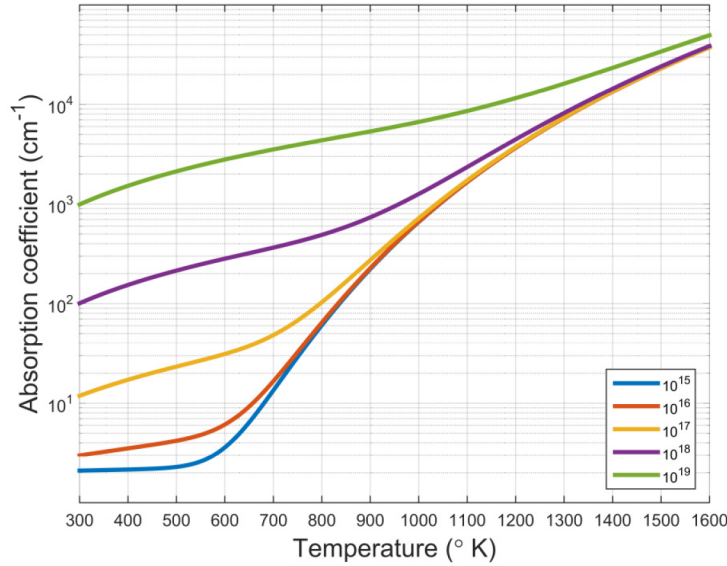

Fig. 1. Calculated optical absorption coefficient of silicon at 10.6μm for different doping levels and temperatures (calculated using the absorption model described in [17]).

The absorption coefficient of diamond at 10.6 μm is quite small and remains below 1 cm^{-1}, even at elevated temperatures around 1000 °K [14]. CVD deposited diamond films have optical properties very similar to single crystal diamond, however optical losses are likely to be somewhat higher in some cases due to scattering from surface roughness and grain boundaries [16]. Since the diamond films of interest in this work are at most a few microns thick, we do not consider absorption in the diamond film, given that the absorption in the highly doped silicon substrate is orders of magnitude higher. It should be noted that graphite, on the other hand, has much higher infrared absorption, but in this work we only focus on modelling the pre-graphitized diamond layer up to the point where graphitization is initiated.

The dominant heat generation process in our structure is due to absorption of the laser beam in the silicon substrate. Optical absorption at 10.6 μm in silicon is mainly due to lattice absorption and free carrier absorption. At 10.6 μm, lattice vibration absorption dominates the absorption mechanism at low temperatures and low doping levels [18]. Intrinsic carrier absorption is temperature dependent, and it dominates the absorption mechanism at elevated temperatures. On the other hand, at high doping levels, doping induced free carrier absorption is the dominant absorption mechanism at low temperatures in extrinsic semiconductors; and for very high doping it becomes comparable to intrinsic carrier absorption at elevated temperatures.

To model the free carrier absorption increase due to thermal effects we use the simplified model described in [17], which is in reasonable agreement with experimentally derived results [18]. The absorption coefficient as a function of doping and temperature can be modeled with the approximate form:

$$\alpha(N,T) = \sigma(T)\left[N + n_i(T)\right] + \alpha_0 \tag{1}$$

where $\sigma(T)$ is the absorption cross-section as a function of temperature in cm^2, N is the extrinsic doping concentration in cm^{-3}, $n_i(T)$ is the intrinsic carrier absorption as a function

of temperature in cm^{-3}, and α_0 is the lattice vibration absorption in cm^{-1}. After substituting the values and equations from [17], the absorption coefficient for n-doped silicon becomes:

$$\alpha(N,T) = \left(1.9 \times 10^{-20} T^{1.5}\right)\left(N + 3.87 \times 10^{16} T^{1.5} e^{\frac{-7020}{T}}\right) + 2 \qquad (2)$$

Calculated absorption curves for various doping levels are shown in Fig. 1. As expected, the curves all converge to a common asymptote at high temperatures, due to the dominance of the thermally generated intrinsic carriers. The behavior for p-doped silicon is qualitatively similar to the n-doped case, however we were not able to find quantitatively reliable optical models in the literature that were backed by experimental data at the wavelength and temperatures of interest.

3. Modelling and simulations

COMSOL Multiphysics was used to model the interaction between the incoming laser beam and a doped silicon substrate with a diamond layer grown on top. The substrate was assumed to have a diameter of 2 inches and a thickness of 380 µm. The mechanical support modelled by a metal heatsink on its lower rim (5 mm overlap between the substrate and heatsink). Steady state simulations were conducted to study the effect of varying the doping concentration, incident laser beam power, and diamond layer thickness on the temperature profile within the structure. Radiative, conductive and convective heat loss mechanisms were all considered, with relevant parameters listed in Tables 1 and 2 in the Appendix. The laser beam was assumed to have a Gaussian profile with a radius of 50 µm. Due to the beam radius being large compared to the wavelength, and the relatively short propagation distance in silicon compared to the Rayleigh range, the beam was assumed to have a constant cylindrical shape throughout the substrate. We used an axisymmetric Beer-Lambert model to simulate the propagation of the laser beam through the wafer. Reflections at the thin film interfaces were modeled using a transfer matrix analysis [19] of the silicon-diamond-air multilayer structure under normal plane wave illumination.

The objective of these simulations is to predict, under various conditions, the attainable temperature of the diamond surface. We assume that once the graphitization temperature (1000 °K) is achieved, the laser assisted chemical etching process will be initiated, resulting in sustained local removal of the diamond film. As mentioned above, we do not attempt to simulate the process past the point of graphitization.

The doping of the substrate has a drastic effect on the laser penetration depth and substrate heating. At low doping levels the optical absorption is low and the beam passes through the wafer, resulting in very little heating. At sufficiently high levels of doping, however, the optical absorption is substantially increased and the beam only penetrates a thin layer near the top surface of the silicon wafer. This creates a hot spot which, in turn, locally increases the number of thermally generated carriers, resulting in even higher absorption and runaway thermal heating.
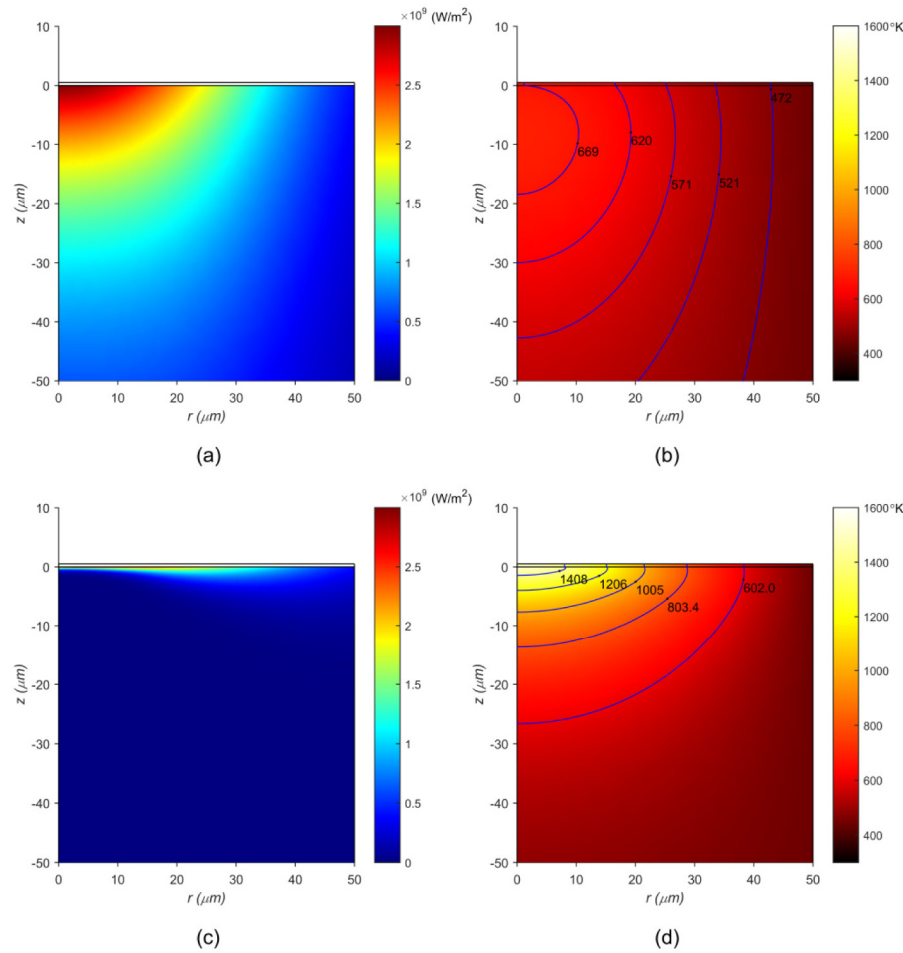
Fig. 2. Simulated laser beam penetration (left) and resulting temperature profiles (right) for silicon substrate doping levels of 10^{18} cm^{-3} (a and b) and 10^{19} cm^{-3} (c and d).

Figure 2 shows two sets of simulations pertaining to these two cases, for a beam power of 15 W. In Fig. 2(a) and Fig. 2(b) the steady state optical intensity distributions and corresponding temperature profiles are shown for an n-type silicon wafer doped at 10^{18} cm^{-3} and covered with a 500 nm diamond layer. As can be seen, the maximum temperature of 670 °K is occurring at a point about 10 microns below the silicon surface. The maximum temperature on the diamond surface is about 1 degree lower (669 °K), which is far below the graphitization temperature.

Figure 2(c) shows the optical intensity distribution for a substrate doped at 10^{19} cm^{-3}. In this case the room temperature optical absorption coefficient is already quite high (about 1000 cm^{-1}, see Fig. 1). The runaway thermal process results in localized heating at the center of beam to about 1500 °K, resulting in an increased local absorption coefficient of 2×10^4 cm^{-1}. The effect of this increase can be seen in Fig. 2(d), where the penetration depth at the center of the beam is smaller than at its edges. In this case the locally generated heat will be more than sufficient to initiate graphitization.

To further explore this effect we carried out a set of simulations over varying beam power and substrate doping. We consider a silicon substrate covered with a 500 nm layer of diamond with n-type doping levels ranging from 10^{16} to 10^{20} cm^{-3}. The color map in Fig. 3 shows the steady state surface temperature of the diamond surface for incoming laser beam powers

varying between 1 and 20 W. As can been seen, at low powers and low doping levels the laser beam is not able to sufficiently heat up the diamond surface to the graphitization temperature. As the doping and laser power are increased, the heat generated by the initial beam absorption is able to create sufficient carriers such that it leads to a runaway buildup of further carriers. The red line in Fig. 3 denotes the boundary beyond which graphitization is initiated. The black area corresponds to points where the temperature exceeds the melting point of the silicon substrate (where our modelling assumptions would be rendered invalid).
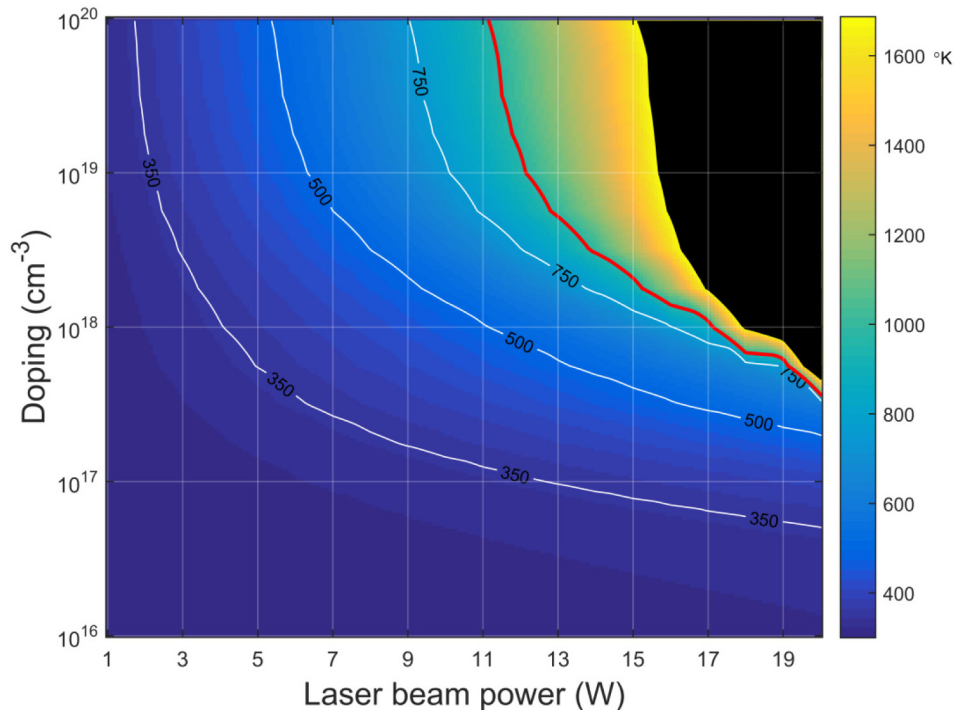

Fig. 3. Maximum diamond surface temperature for different substrate doping and beam power combinations, assuming a 500 nm thick diamond layer doping and a 50 μm beam radius. The red line marks the graphitization threshold temperature of 1000 °K. The black area corresponds to temperatures higher than the melting point of silicon.

As the thickness of the diamond layer is increased, more optical power is required to reach the graphitization temperature on the surface. This is mainly due to increased lateral and longitudinal heat loss in the diamond film as heat is transferred from the hot spot on the silicon surface to the surface of the diamond layer. To investigate this effect we simulated a silicon/diamond structure in the aforesaid mounting and illumination conditions, assuming fixed 10^{19} cm^{-3} doping, the power varying in the range of 12 W to 20 W and the diamond thickness varying between 250 nm and 3 μm. Figure 4 shows the color map corresponding to the steady state temperature of the diamond surface for each of these conditions. As before, the points past (below) the red line correspond to attainment of the surface graphitization temperature and the black area corresponds to temperatures above the melting point of silicon.

This set of simulations show that diamond layers as thick as 2.5 μm can be patterned with CO_2 laser beams under 20W of power, assuming a beam radius of 50 μm. The limit on layer thickness and patterning resolution can be improved by using a more focused beam to create a smaller, more intense, laser beam spot.
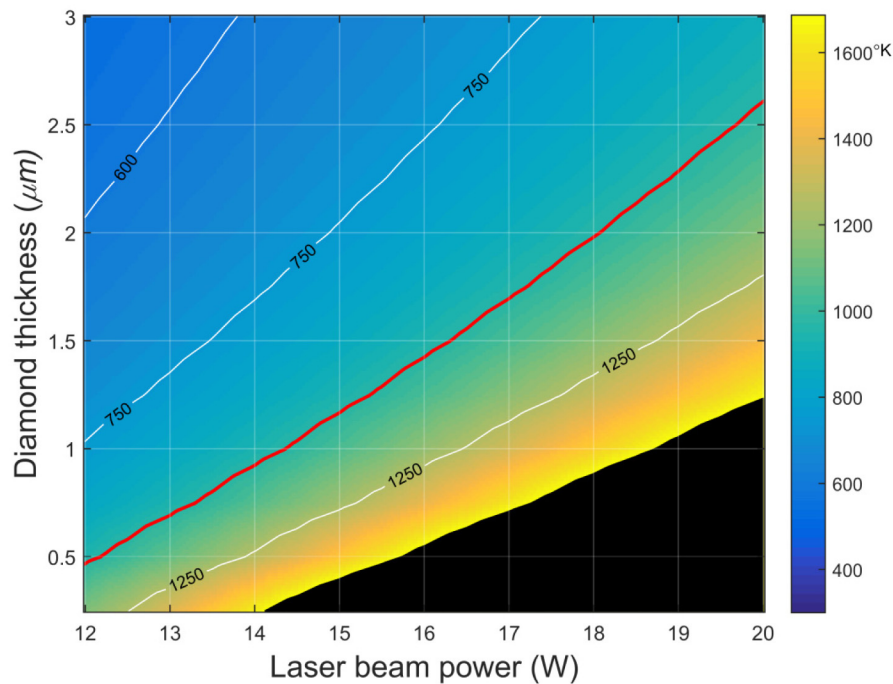
Fig. 4. Maximum diamond surface temperature for different diamond thickness and beam power combinations, assuming a substrate doped at 10^{19} cm^{-3} and a 50 μm beam radius. The red line marks the graphitization threshold temperature of 1000 °K. The black area corresponds to temperatures higher than the melting point of silicon.

4. Experimental results

To demonstrate micromachining of thin film nanocrystalline diamond layers grown on silicon we carried out patterning experiments using a custom-built CO_2 laser micromachining setup. The setup consisted of a CO_2 CW laser (Coherent Diamond C-20A) and a computer controlled 3D positioning stage. The mode quality (M^2) of the emitted beam was specified to be better than 1.2 and the nominal maximum specified optical output power was 20 W, controllable to a precision of approximately 50 mW. In practice a slightly higher optical output power of about 22 W was achievable. The laser beam was focused down to a spot with a beam radius of approximately 130μm by the use of a biconvex zinc selenide lens with a focal length of 100 mm. An image acquisition system performed live capture and control of the illumination process of a sample.

The sample used in the experiments consisted of a nanocrystalline diamond film grown on a 380μm thick silicon wafer highly doped with boron. The surface conductivity of the wafer was measured to be 79.4 mΩ/□ using a four point probe measurement system (Jandel, 1mm probe spacing). This translates to a conductivity of 0.003 Ω-cm and a doping level of 3.7 × 10^{19} cm^{-3}. The diamond film was grown from monodispersed hydrogenated diamond nanoparticles using chemical vapor deposition in a microwave plasma reactor with methane and hydrogen gases [20]. The growth conditions were set to (CH_4:5 sccm, H_2:475 sccm, Power: 3500 W, Pressure: 40 Torr) at a temperature of 842°C, for a growth duration of 298 minutes, resulting in a 600 nm unpolished film. The film grain size was not measured before polishing, however the grain sizes are estimated to be in the range of 150-300 nm, inferred from the growth conditions and similarly grown samples [20]. Detailed information on the effect of growth parameters on the film morphology can be found in [21]. The film was polished using chemical mechanical polishing down to an average thickness of 520nm and a surface roughness less than 2 nm (RMS).
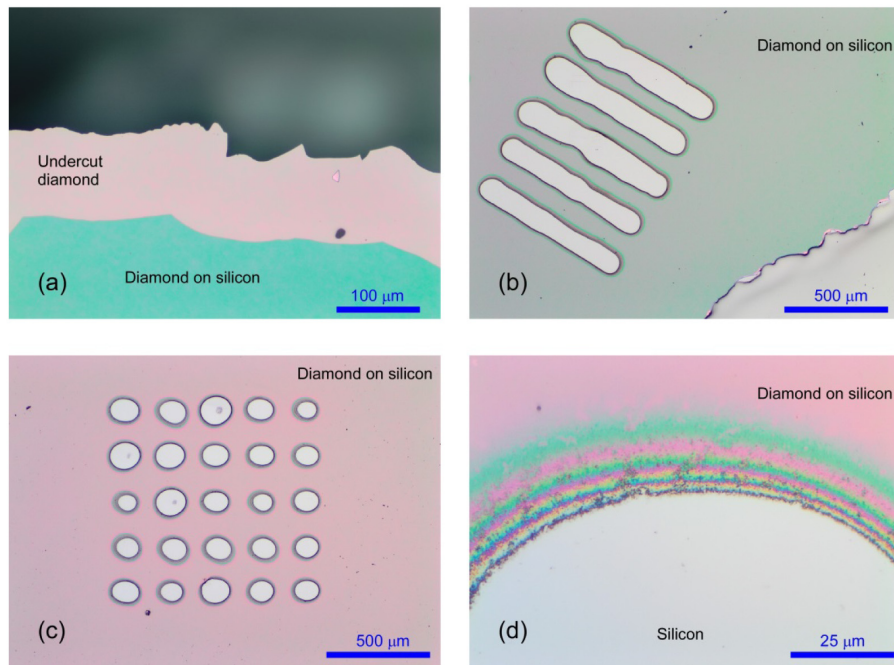
Fig. 5. (a) Undercut nanocrystalline diamond film on silicon substrate. Lines (b) and dots (c) patterned in diamond. (d) Zoomed-in image of a dot showing interference fringes and debris.

The chip was supported on a horizontal metal platform with a beam exit hole, without the use of any additional heatsinking compounds. The diamond film on the chip edge was undercut and released using a XeF_2 silicon dry etch (Fig. 5(a)). The absence of ripples in the undercut membrane indicates very little residual stress in the diamond film. Exposure of this section of the chip to a focused CO_2 laser beam did not result in any perceptible changes in the film appearance, even at high powers up to 20 W. This confirms the very low absorption coefficient of the diamond film at 10.6 µm. However, when the beam was directed to sections with an underlying silicon layer, the diamond film was rapidly removed at beam powers above 9 W (with a beam radius of ≈130 µm), resulting in a clean and unblemished exposed silicon surface. The beam intensity levels required for patterning the diamond film in our experiment are lower than the levels predicted by the simulations. We attribute this to the smaller size of the actual chip compared to the full 2 inch wafer used in the simulations and also use of an ideal heat heatsink boundary condition in the simulations. In practice we also observed that points closer to the chip edge were machined faster and at lower power levels compared to the center of the chip, which is due to the difference in the heat loss parameters at these points.

It may be argued that initiation of the diamond etch process could also be due (in part, or fully) to surface absorption processes in the diamond film. These would consist of absorption at the nanocrystal diamond surfaces on the air/diamond interface and a silicon carbide layer (< 1nm thick) existing on the silicon/diamond interface. However, both of these surface effects would also be present in the suspended diamond film, since silicon carbide is not etched in XeF_2 gas. Since the experiments show that the suspended diamond film is not affected by the incoming laser beam, we can conclude that the heating effect of any surface absorption in the diamond film is negligible compared to the heat generated through absorption in the silicon substrate.

Using the automated stage controls, arrays of dots and lines were written into the diamond film (Figs. 5(b), 5(c)). Closer inspection of the patterned areas shows interference fringes,

indicating a gradual increase in the film thickness away from the etched diamond edge. Also, some dark micron-scale and sub-micron-scale particles can be seen in the periphery of the etched edge which are possibly residual graphite or diamond nanoparticles generated during the heating process.

It should be mentioned that the focused CO_2 laser beam was not optimized for achieving the smallest focused spot size and we expect that a patterning resolution substantially higher than shown in Fig. 5 should be achievable in practice. In the ideal case of a diffraction limited spot, assuming a numerical aperture of unity, a focused CO_2 laser beam would have a spot diameter of $2w_0 = \frac{2\lambda_0}{\pi} = 6.8$ µm, which is about 40 times smaller than the spot size used in the experiments. Additional improvement in resolution can also be achieved by using a high power laser source with a shorter wavelength, such as a fiber laser operating in the near IR. It should however be noted that free carrier absorption in silicon is approximately proportional to the square of the wavelength [18], therefore operating at shorter wavelengths will require higher laser powers and substrate doping levels in order to reach the graphitization temperature.

5. Conclusion

Through simulations and experiments we have demonstrated that under the right substrate doping conditions, a thin diamond film grown on a silicon wafer can be patterned with a CO_2 laser beam at modest optical power levels. Our simulations show that the presence of the substrate and its doping level play a crucial role in this process, a fact that seems to have been unnoticed in previous work done in this area. Our work demonstrates that patterning of diamond can be achieved without directly graphitizing the diamond surface with high peak-power pulsed lasers. This in turn opens up the possibility of using industrial CW CO_2 lasers for micromachining diamond films. The results can also be relevant to laser micromachining of other types of transparent thin film material systems grown on silicon substrates. In addition, the substrate heating effect described here is not necessarily limited to the case of CW laser machining and can play a significant role in analyzing the processes involved in high peak power pulsed laser machining of diamond thin films.

Appendix A:

Details of relevant physical parameters used in the COMSOL modelling steps.

Table 1. Silicon parameters

Parameter	Value	Units	Comment
Density	$\rho(T) = 2330 - 2.19 \times 10^{-2}(T - 293.15)$	Kg/m^3	From [22].
Heat Capacity	$C_p(T) = 641 + 74.2\dfrac{T}{300}$	$J/(Kg°K)$	From [23].
Thermal conductivity	$k(T) = 156 \times \left(\dfrac{T}{300}\right)^{-4/3}$	$W/(m°K)$	After modifying the equation in [23], also the effect of doping on thermal conductivity has been ignored.
Emissivity	0.5		Using average value from [24].

Table 2. Diamond parameters

Parameter	Value	Units	Comment
Density	3515	Kg/m^3	From [14].
Heat Capacity	$C_p = 3T - 400$	$J/°K$	Extrapolated and extended from [14].
Thermal conductivity	$k = \dfrac{2.833 \times 10^6}{T^{1.245}}$	$W/(m°K)$	From [25].
Emissivity	0.03		Average value from [25].

Funding